fibers

MDPI

Article

Synergistic Effect of HEDP.4Na and Different Induced Pouring Angles on Mechanical Properties of Fiber-Reinforced Alkali-Activated Slag Composites

Jingjie Wei [1,2], Jianwei Liu [1], Kamal H. Khayat [2] and Wu-Jian Long [1,*]

[1] Guangdong Provincial Key Laboratory of Durability for Marine Civil Engineering, Key Laboratory of Coastal Urban Resilient Infrastructures, MOE, College of Civil and Transportation Engineering, Shenzhen University, Shenzhen 518060, China

[2] Advanced Construction and Material Laboratory, Center of Infrastructure Engineering Studies, Department of Civil, Architectural and Environmental Engineering, Missouri University of Science and Technology, Rolla, MO 65401, USA

* Correspondence: longwj@szu.edu.cn

Abstract: The poor flexural and damping properties of building materials damages concrete structures and affects their service life when concrete structures are subjected to dynamic loads. Three different dosages (i.e., 0%, 0.3%, and 0.6%) of organic phosphonates (HEDP.4Na) and different pouring methods (i.e., conventional pouring method, 90°-induced pouring method, and 150°-induced pouring method) were designed to improve the flexural and damping performance of fiber-reinforced alkali-activated slag composites (FR-AASC). The enhanced mechanism of HEDP.4Na was revealed by phase analysis (X-ray diffraction, XRD), pore structure analysis (Mercury Intrusion Porosimetry, MIP), the heat of hydration, and scanning electron microscopy (SEM) analysis. The results showed that 0.3% HEDP.4Na combined with the 150°-induced pouring angle can significantly improve the mechanical properties of the FR-AASC sample compared with the reference group. The sample with 0.3% HEDP.4Na cast by the 150°-induced pouring angle increased compressive and flexural strength, damping energy consumption and storage modulus by 20%, 60%, 78%, and 30%, respectively, compared with the reference sample cast by the conventional pouring methodology. HEDP.4Na reduced the early hydration heat and total porosity of the FR-AASC matrix, modified the fiber–matrix interface transition zone, and increased the frictional energy consumption of steel fibers. Overall, the synergistic effect of HEDP.4Na and the induced pouring methodology significantly improved the flexural and damping properties of FR-AASC. This study can provide a guidance for improving the flexural and damping capacity of FR-AASC and promote the application of FR-AASC in construction engineering.

Keywords: fiber-reinforced alkali-activated slag composites; compressive strength; flexural strength; damping performance; microstructure

Citation: Wei, J.; Liu, J.; Khayat, K.H.; Long, W.-J. Synergistic Effect of HEDP.4Na and Different Induced Pouring Angles on Mechanical Properties of Fiber-Reinforced Alkali-Activated Slag Composites. *Fibers* **2023**, *11*, 23. https://doi.org/10.3390/fib11030023

Academic Editor: Anastasios C. Mpalaskas

Received: 7 December 2022
Revised: 15 February 2023
Accepted: 20 February 2023
Published: 22 February 2023

1. Introduction

Ordinary Portland cement concrete is the most widely used building material, and its annual yield in the world has exceeded 6 billion tons (about 1 ton/year/person) [1]. Ordinary Portland cement (OPC) is one of the main components of concrete, accounting for 10–12% of the total volume of concrete [2]. Currently, more than 4 billion tons of cement are produced per year, accounting for around 8% of global CO_2 emissions [3]. According to the report of the global cement and concrete association in 2021, the cement industry needs to decrease CO_2 emissions by 25% by 2030 and become net zero until 2050 to meet the requirements of the Paris Agreement regarding climate change [4]. However, the demand for concrete still increases yearly with the rapid development of infrastructure construction. For example, it is estimated that 1.53 m^3 (2 yd^3) of concrete per person is placed each year

to support the U.S. infrastructure [5]. The consumption of cement in the United States (U.S.) has steadily increased since 2008, reaching approximately 102 million metric tons in 2019 [6]. Therefore, a new type of concrete material should be developed to decrease the environmental impact of concrete, while taking performance into consideration.

Alkali-activated slag composites (AASC) are a class of green and low-carbon building materials synthesized by the chemical reaction between alkaline solution and aluminosilicate. Compared with OPC, AASC can reduce CO_2 emissions by 50–80%, decrease energy consumption by 60%, and show better compressive performance and high durability [7–9]. However, AASC has several main shortcomings, such as low fluidity and short setting time [10,11]. For example, Fang et al. [12] reported that the average initial and final setting time was 0.9 and 1.5 h when the dosage of Na_2O was 6% in the AASC mixture, while the initial and final setting time of the OPC mixture was over 6 and 12 h. According to previous studies [13,14], the AASC cannot be applied to concrete structures that require high flexural strength and strong damping capacity. For example, Long et al. [13] compared the damping capacity of mortar phase made with different binder systems, showing the damping capacity of AASC mortar was lower than those made with other binder systems. Similar results were also reported by the investigation of Zhu et al. [15], showing that the damping capacity of fly ash-based geopolymer was 30% lower than OPC specimens. However, concrete structures are usually subjected to dynamic loads (earthquake, wind, vehicle loads, etc.) during their service life [16,17]. It is well known that an improvement in the damping performance from the material level, combined with effective structural seismic design, not only reduces the damage of dynamic loads to the structure but also improves the safety and comfort of the structure during its service life. The enhancement of the damping performance of building materials can make the concrete structure consume more energy at the material level, thereby reducing the amplitude and stress and improving the damping of the overall concrete structures [18,19].

Chi et al. [20] reviewed the damping capacity of cement matrix composites at the material level and summarized various additives to enhance the damping capacity of cement matrix composites. Among these additives, steel fibers can be used to improve the mechanical properties, including flexural and damping properties, of cementitious composites because steel fibers can transfer tensile stress from the matrix, resist crack propagation, and improve the toughness of the matrix [21–24]. However, Swamy et al. found that the utilization of steel fibers in improving the flexural properties of composites is severely limited [25]. Based on the principle of tensile stress in fiber-reinforced composites, the efficiency of steel fibers in improving the performance of cement-based composites in uniaxial mechanical tests is only 30% due to the random orientation of fibers in the cement-based composites [26,27]. The orientation and uniform distribution of steel fibers are of great significance in enhancing the flexural properties of cement-based composites. For example, Ferrara et al. [28] and Teng et al. [29] cast beams in which the orientation of the fibers dominates in the principal tensile direction, thereby significantly increasing the bearing capacity of the beams. Huang et al. [22] used an L-shaped device to increase the fiber orientation of beams, which increased the flexural strength by 65% compared to the samples cast by the traditional method. Zhang et al. [30] reported that the ultimate tensile strength of the samples cast using channels with vibrations increased by 66% compared to the reference sample cast by the conventional pouring method. However, these studies mainly aimed improve the mechanical properties of ordinary cement composites, while the research on improvement in damping and flexural performance in AASC is relatively limited. The fresh properties (i.e., mini-slump flow and setting time) of AASC showed a significant difference from the ordinary cement composites, which influenced the efficiency of steel fibers in improving the mechanical performance of AASC. Gou et al. [31] developed a novel device to orientally distribute fine and short steel fibers in the cement mortar, producing excellent stress-dispersing (flexural strength) and absorbing effects (toughening). Teng et al. [32] compared different casting methods to investigate the flexural performance of cement-based composites, indicating that the casting method significantly influenced

the flexural performance of specimens. It indicates that the casting method could influence the hardened performance of samples. However, the current research method does not consider the effect of different pouring angles on the flexural and damping properties of fiber-reinforced AASC (FR-AASC).

Tetrasodium salt of 1-hydroxyethylidene-1,1-diphosphonic acid (HEDP.4Na) is an excellent metal corrosion inhibitor widely used in chemical, metallurgical, and other industrial water treatments [19,33]. It can dissolve various metal oxides and form stable complexes. Currently, HEDP.4Na has been applied in cement-based composites, including OPC, magnesium oxysulfate cement (MOC), and oil well cement. Liang et al. [34] reported that HEDP.4Na can promote the formation of the needle-shaped crystals phase in the MOS cement system and improve the compressive strength and softening coefficient of MOS cement. Hurnaus et al. [35] studied the use of organic phosphonic acid compounds as retarders to maintain the fluidity of concrete, reporting that organic phosphonic acid compounds improve the fluidity properties. The speed of polymerization in AASC mainly depends on the combined rate of Ca^{2+} dissolved in slag and silicate ions. If HEDP.4Na is introduced into the AASC system, it may form a stable complex with Ca^{2+} ions to cover the surface of the slag and inhibit the polymerization reaction in AASC. Therefore, the fresh performance, including slump flow and setting time, may be modified through the addition of HEDP.4Na. According to the existing research, the variation in the fresh performance of the paste greatly affects the hardening performance of FR-AASC [36,37]. However, there are limited studies on FR-AASC concerning the effect of HEDP.4Na on the flexural and damping properties.

Based on the aforementioned literature review, a new type of concrete material should be developed to decrease the environmental impact of concrete while taking flexural and damping performance into consideration. The current research method does not consider the effect of different pouring angles and HEDP.4Na on the flexural and damping properties of fiber-reinforced AASC (FR-AASC). In this study, to improve the mechanical properties of FR-AASC, the effect of different dosages (mass ratio to cement: 0%, 0.3%, 0.6%) of HEDP.4Na and different pouring methods (conventional pouring method, 90°-induced pouring method, 150°-induced pouring method) on compressive strength, flexural strength, and damping properties of AASC were studied. An acme penetrometer and slump flow cone were used to investigate the effect of HEDP.4Na on the setting time and slump flow of FR-AASC. Additionally, phase analysis (XRD), the heat of hydration, mercury intrusion porosimetry (MIP), and scanning electron microscopy (SEM) were measured to reveal the influenced mechanism of HEDP.4Na on the flexural and damping properties of FR-AASC. This research can provide certain guidance for improving the flexural and damping performance of FR-AASC and lay an important theoretical foundation for future architectural applications.

2. Experimental Materials and Methods

2.1. Raw Materials

In this study, the alkali activator consisted of a sodium hydroxide (NaOH) and sodium silicate (Na_2SiO_3) solution. Sodium hydroxide (analytical purity 96%) was produced by Shanghai Api Chemical Reagent Co., Ltd. (Shanghai, China), and the appearance was white crystalline flakes. The sodium silicate solution (SS, SiO_2/Na_2O molar ratio = 3.34, water content = 62.3%) was supplied by Wuhan Xinchuyang Chemical Co., Ltd. (Wuhan, China), and the appearance was a transparent and viscous liquid. The S95 blast furnace slag (GGBFS), provided by Shanghai Weishen New Building Materials Co., Ltd. (Shanghai, China), was used as the activated cementitious material. The river-bed siliceous sand with a maximum particle size of 4.25 mm, fineness modulus of 2.62, a specific gravity of 2.59, and surface saturated dry water absorption of 0.38% was used as fine aggregate. The main chemical composition of CaO, SiO_2, and Al_2O_3 content were 40%, 33%, and 17%, respectively, and the specific surface area was 430 $kg.m^{-2}$. HEDP.4Na, a white powder soluble in water produced by Guangzhou Deli Chemical Co., Ltd. (Guangzhou, China),

was used to modify the fresh properties of FR-AASC. The physical properties of HEDP.4Na are shown in Table 1. The dosage of HEDP.4Na in FR-AASC was 0.0%, 0.3%, and 0.6% of the mass of the cementitious material. The diameter, length, and tensile strength of the selected steel fiber were 0.2 mm, 13 mm, and 2790 MPa, respectively.

Table 1. Physical characteristics of HEDP.4Na.

Property	Morphology	HEDP Content/wt%	Purity/wt%	Density/g.m^2	pH
HEDP.4Na	White powder	≥65.0	≥90.0	1.26–1.36	11.0–12.0

2.2. Mixture Design and Specimen Preparation

The mixture proportions of FR-AASC are shown in Table 2. To ensure the workability of the FR-AASC, the water–binder ratio (W/B) and volume of steel fibers in this study were fixed at 0.45 and 1 vol.%. Different contents of HEDP.4Na (0%, 0.3%, and 0.6% by mass of cementitious materials) were added to control the fresh performance of the FR-AASC mixtures. The mixing procedure was as follows: (1) NaOH was dissolved into water, stirred with Na_2SiO_3 solution for 3 min, then covered with plastic wrap for 30 min; (2) HEDP.4Na powder was added to the mixed solution of NaOH and Na_2SiO_3, and then stirred for 3 min; (3) the slag and fine aggregate were mixed in a mixer at low speed for 30 s, and then the mixed solution was added to the FR-AASC mixture, followed by 2 min of low-speed and 2 min of high-speed mixing; (4) the steel fibers were incorporated into the mixture and mixed for 2 min at a low-speed rate. The mini-slump flow of the FR-AASC was evaluated using a mini-slump cone with a height of 60 mm, a top inner diameter of 70 mm, and a bottom inner diameter of 100 mm. Different pouring methods, including the conventional pouring method and 90°- and 150°-induced pouring angle methods, were used to cast FR-AASC samples into the mold with a dimension of 100 mm × 100 mm × 405 mm for the flexural test, as shown in Figure 1. The FR-AASC samples with a dimension of 100 mm^3 were cut from flexural samples with the dimension of 100 mm × 100 mm × 405 mm for compressive strength tests. All FR-AASC specimens were cured in a standard curing room with a temperature of 20 ± 2 °C and humidity of >95% for 28 days after 24 h of de-molding.

Table 2. Mixture proportions of FR-AASC.

Specimen	GGBFS kg·m^{-3}	Sand kg·m^{-3}	NaOH kg·m^{-3}	Na_2CO_3 kg·m^{-3}	Water kg·m^{-3}	Steel Fiber vol.%	HEDP.4Na Mass%	Induced Pouring Angle (°)
HEDP-0-Ref.	1000	1500	19.27	77.05	400	1	0	Ref.
HEDP-0-90°	1000	1500	19.27	77.05	400	1	0	90°
HEDP-0-150°	1000	1500	19.27	77.05	400	1	0	150°
HEDP-0.3%-Ref.	1000	1500	19.27	77.05	400	1	0.3	Ref.
HEDP-0.3%-90°	1000	1500	19.27	77.05	400	1	0.3	90°
HEDP-0.3%-150°	1000	1500	19.27	77.05	400	1	0.3	150°
HEDP-0.6%-Ref.	1000	1500	19.27	77.05	400	1	0.6	Ref.
HEDP-0.6%-90°	1000	1500	19.27	77.05	400	1	0.6	90°
HEDP-0.6%-150°	1000	1500	19.27	77.05	400	1	0.6	150°

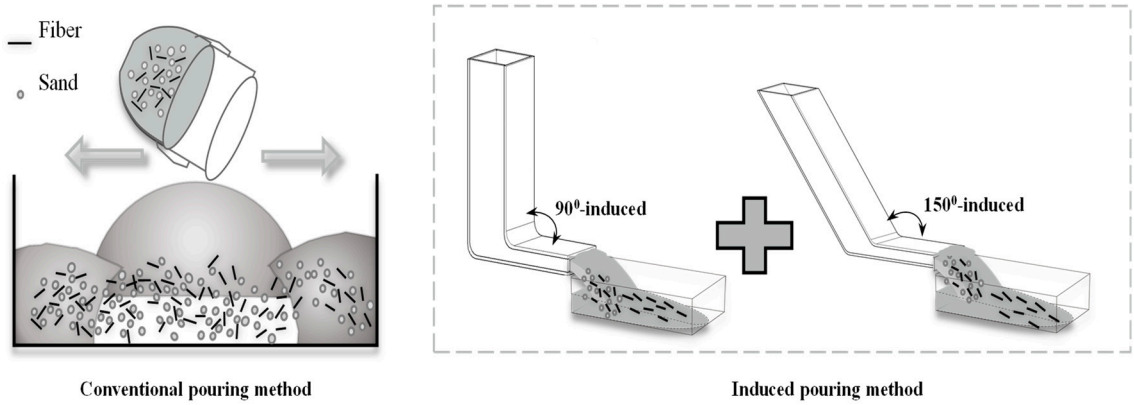

Figure 1. Different casting methods.

2.3. Test Method

2.3.1. Mini-Slump Flow and Setting Time

The workability and consistency of the FR-AASC mixtures play a critical role in ensuring concrete quality in a construction project. The mini-slump test was conducted according to the standard of ASTM C230/230M [38]. The FR-SWC mixtures were filled into a mini-slump cone with a height of 60 mm, an upper inner diameter of 70 mm, and a bottom inner diameter of 100 mm. The mini-slump cone was lifted vertically to allow the FR-AASC mixtures to flow. The mini-slump flow of the FR-AASC mixtures was determined by the average value of two directions perpendicular to each other. Additionally, the setting time of the mortar phase from the FR-AASC mixtures was measured according to the standard of ASTM C403 [39]. A mortar phase of FR-AASC was placed in a container with a dimension of 40 mm × 80 mm and then stored at a specified laboratory condition with a temperature of 23 ± 3 °C and a relative humidity of 50 ± 5%, respectively. The resistance of the mortar to penetration by standard needles was measured at constant time intervals.

2.3.2. Compressive and Flexural Strength Test

Compressive and flexural strength tests are widely accepted methods to evaluate the performance of a given FR-AASC mixture. To evaluate different HEDP.4Na contents and different pouring methods on the mechanical behavior, including compressive and flexural strength, of FR-AASC samples, a 200-ton electro-hydraulic servo pressure tester was used to determine the 28-day compressive strength of the sample. The parameter setting during the experiment was accordance in with ASTM C109 [40]. The loading rate was set at 2.4 kN/s. According to AASTM C1609 [41], a loading rate of 2 mm/min was used to evaluate the 28-day flexural strength of all FR-AASC beams with a span of 300 mm.

2.3.3. Dynamic Mechanical Properties Test

According to the investigation by Long et al. [42,43], the dynamic performance of FR-AASC was tested using a dynamic thermomechanical analyzer (DMA+1000) produced by Metravib (Paris, France). The DMA samples with a dimension of 30 mm × 30 mm × 100 mm were obtained by cutting the center of the prism. According to previous experimental studies [44,45], low-frequency waves of earthquakes or vibrations of 0.5~2.5 Hz are likely to cause dynamic damage to concrete structures. Therefore, the damping characteristics and storage modulus of FR-AASC were tested for 28 days at room temperature (25.3~25.5 °C) and an excitation frequency of 0.5~2.5 Hz.

2.3.4. Phase Analysis

Phase analysis of the FR-AASC samples was tested using an X-ray diffractometer (XRD), manufactured by Bruker Optics, Germany. The sample powder was obtained from the crushed sample after filtering fine aggregates and steel fibers and further grinding

through a 200-mesh sieve for XRD measurement. The XRD analysis was performed by XRD equipped with monochromatic Cu-Ka radiation at 40 kV and 40 mA. The scan was initialized at 0.02° with a scan rate of 2/min.

2.3.5. Heat of Hydration Analysis

The heat of hydration, heat flow, and cumulative heat of hydration of FR-AASC were monitored using a physical property calorimeter provided by TA Instruments. The temperature in the measurement channel was kept constant at 20 ± 0.1 °C. The time interval of hydration heat data collection was 24 s, and the total measurement time was 72 h.

2.3.6. Pore Structure Analysis

The pore size distribution and porosity of the mortar phase of FR-AASC were evaluated using a mercury porosimeter (MIP, Auto Pore IV 9500) produced by Micromeritics Instruments Corporation (Norcross, GA, USA). The FR-AASC specimens were crushed into small particles with a dimension of 3~6 mm, and then dried in an oven at 65 °C for 24 h before MIP tests. The full-scan auto mode was selected with a contact angle of 130° and surface tension of 485 mN/m, respectively. The MIP tests were sequentially conducted under low pressure (345 kPa) and high pressures (420 MPa), respectively.

2.3.7. Scanning Electron Microscopy (SEM) Analysis

The 28-day FR-AASC samples were impregnated with epoxy resin, and then slowly cut with a high-precision cutting machine. The obtained FR-AASC samples were oven-dried and then characterized by a Quanta-200FEG electron microscope (FEI Company, Hillsboro, OR, USA). The working voltage was 20 Kv, and the image pixels were 1280 × 960.

3. Results and Discussion

3.1. Setting Time and Mini-Slump Flow of FR-AASC

The setting time and mini-slump flow of FR-AASC incorporated with various HEDP.4Na contents are shown in Figure 2. The initial and final setting times of FR-AASC without HEDP.4Na were 30 and 65 min, respectively, while the initial and final setting times of AASC containing 0.3% and 0.6% HEDP.4Na were 40 and 48 min, 100 and 85 min, respectively. It can be observed that the FR-AASC mixtures containing HEDP.4Na significantly delayed the initial and final setting times compared to the FR-AASC mixture without HEDP.4Na4. As the HEDP.4Na content increased from 0% to 0.3%, the initial and final setting times of the FR-AASC mixture were delayed by 43.8% and 42.0%, respectively. The FR-AASC mixture containing 0.6% HEDP.4Na delayed the initial and final setting times by 25% and 17%, respectively, compared to the FR-AASC without HEDP.4Na. Similar results were reported by Liang et al. [34], showing that MOC with 0.75% HEDP delayed the setting time by 150% compared to the control sample.

It Is well known that prolonging the initial setting time can increase the slump flows of the FR-AASC mixture [46]. In this study, the variation in mini-slump flow for the FR-AASC mixtures showed a similar tendency to the initial setting time. HEDP.4Na significantly improved the mini-slump flow of the FR-AASC mixtures. As shown in Figure 2, the mini-slump flow of the FR-AASC mixtures containing 0.0%, 0.3%, and 0.6% HEDP.4Na was 180 mm, 230 mm, and 215 mm, respectively. The use of 0.3% and 0.6% HEDP.4Na in the FR-AASC mixtures increased the min-slump flow by 18% and 27% compared with the control group without HEDP.4Na. Similar results were reported in the literature [34], displaying that MOS cement with 0.5%HEDP increased the slump flow by 30% compared to the control mixture. This was also consistent with the previous study [47]. The reason was that HEDP.4Na decomposed into $HEDP^{4-}$ and $4Na^{-}$ after being dissolved in an aqueous solution and then combined with $2Ca^{2+}$ ions from the slag to form HEDP.2Ca [48]. The product of HEDP.2Ca can inhibit the polymerization reaction of Ca^{2+} ions dissolved in the slag and silicate, reducing the rate of the alkali-activated polymerization reaction and indirectly improving the mini-slump flow of FR-AASC.

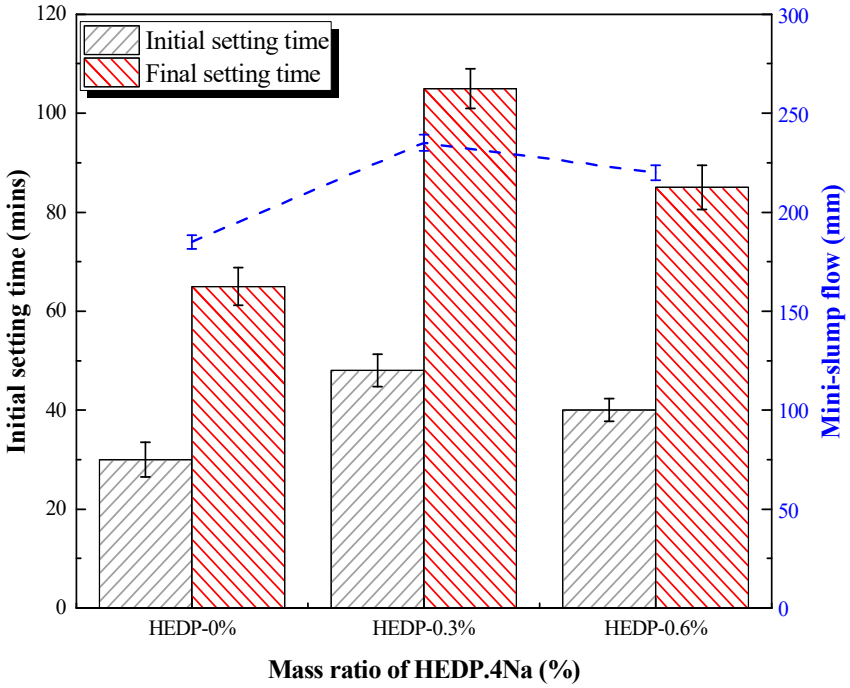

Figure 2. Effect of HEDP.4Na on setting time and mini-slump flow.

3.2. Compressive Strength of FR-AASC

Figure 3 shows the effect of different HEDP.4Na contents and different induced pouring methods on the 28-day compressive strength of FR-AASC samples. The FR-AASC samples incorporated with 0.3%HEDP.4Na (HEDP-0.3%) cast by different pouring methods increased the 28-day compressive strength by 14–20% compared to the control sample (HEDP-0%). Similar results were reported by Kiiashkio et al. [48], showing that HEDP-0.4% increased the 28-day compressive strength of Na_2CO_3-activated slag composites by 20–25%. This was attributed to the mini-slump flow of HEDP-0.3% being significantly higher than that of the reference group. The increase in the mini-slump flow of FR-AASC increased the internal compactness of the hardened FR-AASC matrix. The high compactness of the matrix finally improved the 28-day compressive strength of FR-AASC samples, which was also consistent with the tested results of MIP in Section 3.7. The HEDP-0.6% sample slightly decreased the 28-day compressive strength by 4% compared to the HEDP-0.3% sample, although the 28-day compressive strength increased by 17% compared to the control sample. This result indicated that there is an optimal dosage of HEDP.4Na, and the excessive dosage of HEDP-4Na slightly decreased the compressive strength of FR-AASC compared with the HEDP-0.3% sample. Another reason may be that the precipitation of HEDP.2Ca covering the surface of the hydration product inhibits the formation of C-A-S-H-gelling materials, thereby reducing the compressive strength of the matrix [49]. Furthermore, Figure 3 shows that the FR-AASC samples prepared by the induced pouring method slightly increased the 28-day compressive strength by 5% compared with the FR-AASC sample cast by the conventional pouring method. The induced pouring method improved the steel fibers' distribution in the matrix and enhanced the 28-day compressive strength of FR-AASC, which is consistent with the findings of Huang et al. [22].

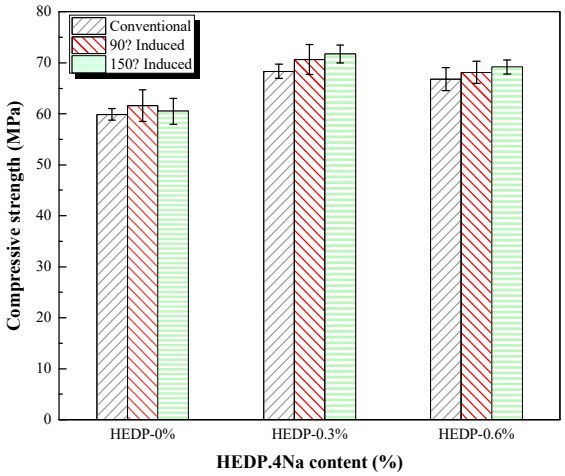

Figure 3. Compressive strength of 28d FR-AASC.

3.3. Flexural Strength of FR-AASC

The effect of different HEDP.4Na contents and different induced pouring methods on the 28-day flexural strength of the FR-AASC are shown in Figure 4. Using three different pouring methods to prepare samples, it can be observed that the HEDP-0.3% and HEDP-0.6% samples increased the 28-day flexural strength by 14–45% and 23–33%%, respectively, compared with the control sample. This indicated that HEDP.4Na can significantly enhance the flexural performance of FR-AASC. It was attributed to the fact that HEDP.4Na can modify the interface transition zone between steel and AASC matrix, verified by the SEM analysis in Section 3.9. Additionally, the induced pouring method can significantly improve the flexural strength of FR-AASC compared with the conventional pouring method. Compared with the FR-AASC beam cast by the conventional method, a maximum value of 14.9 Mpa in flexural strength for the FR-AASC samples cast by the 150°-induced pouring method was obtained. The HEDP-0.3% sample cast by the 150°-induced pouring method increased the 28-day flexural strength by 60% compared with the reference sample cast by the conventional pouring method. The increase in flexural strength of FR-AASC was with respect to the angle between the steel fibers and the main tensile stress. Therefore, the 150° pouring method significantly enhanced the alignment of steel fibers in the AASC matrix compared to other pouring methods. Similar results were reported by Teng et al. [50], showing that the enhancement efficiency of steel fibers in the flexural resistance of ultra-high-performance concrete beams can be significantly improved by 45% when the alignment of the steel fiber is the same as the tensile stress.

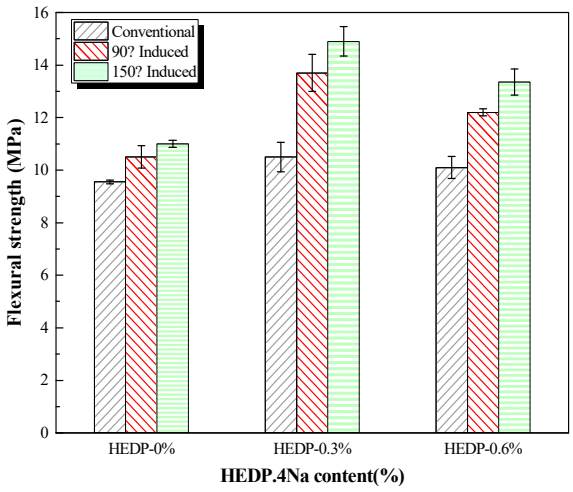

Figure 4. Flexural strength of 28d FR-AASC.

3.4. Loss Factor of FR-AASC

The damping performance of a material can be characterized by the parameter loss factor, according to previous studies [44,51,52]. Figure 5 shows the 28-day loss factor of the FR-AASC samples incorporated into different HEDP.4Na contents and cast by various pouring methods. It can be observed that the loss factor of FR-AASC at 0.5~2.5 Hz was steady and did not change with time. It indicated that the loss factor of FR-AASC is not sensitive to the variation in frequency and time. However, HEDP.4Na can significantly improve the loss factor of FR-AASC. For a given excitation frequency of 0.5 Hz, the HEDP-0.3% and HEDP-0.6% samples increased the loss factor by 52% and 30%, respectively, compared with the control sample. This was mainly attributed to the fact that HEDP.4Na can improve the fluidity of the FR-AASC mixture, enhancing the inner compactness of the FR-AASC specimens. Additionally, an appropriate dosage of HEDP.4Na can promote the hydration of C-A-S-H gel in FR-AASC at the late stage, modifying the interface transition zone of the steel fiber–AASC matrix and contributing to the energy dissipation of FR-AASC. Similar results were reported by Giner et al. [53], showing that the addition of silica fume modified the interface between carbon fiber and concrete matrix and improved the damping ratio of concrete by 6% compared to the control specimen.

The loss factor of FR-AASC was significantly affected by various pouring methods. For a given excitation frequency of 0.5 Hz and HEDP.4Na content, the FR-AASC samples cast by 90° and 150° pouring methods increased the loss factor by 12% and 17%, respectively, compared with the traditional pouring method. Furthermore, the HEDP-0.3% sample cast by the 150°-induced pouring method increased the loss factor by 78% compared with the reference sample prepared with the conventional pouring methodology. Furthermore, the improved efficiency of the induced pouring method in the energy dissipation capacity was lower than that of HEDP.4Na. The improvement in the loss factor in FR-AASC using the induced pouring method was mainly due to the optimization of the fiber distribution and alignment in the matrix. Steel fibers generated great tensile stress under the external dynamic load to inhibit crack propagation when steel fibers were aligned with the direction of tensile stress. The increase in friction slips between the steel fibers and the AASC matrix ultimately enhanced the energy dissipation of FR-AASC. The increase in the compactness of the FR-AASC matrix weakened the deformation ability under the external dynamic load. However, the uniform fiber distribution and the enhancement of the interface transition zone between steel fibers and matrix can offset the negative effect [13].

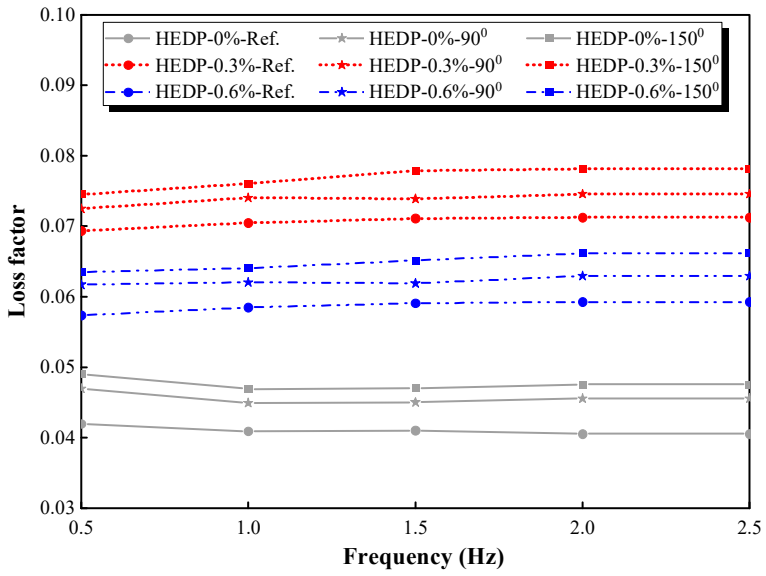

(**a**)

Figure 5. *Cont.*

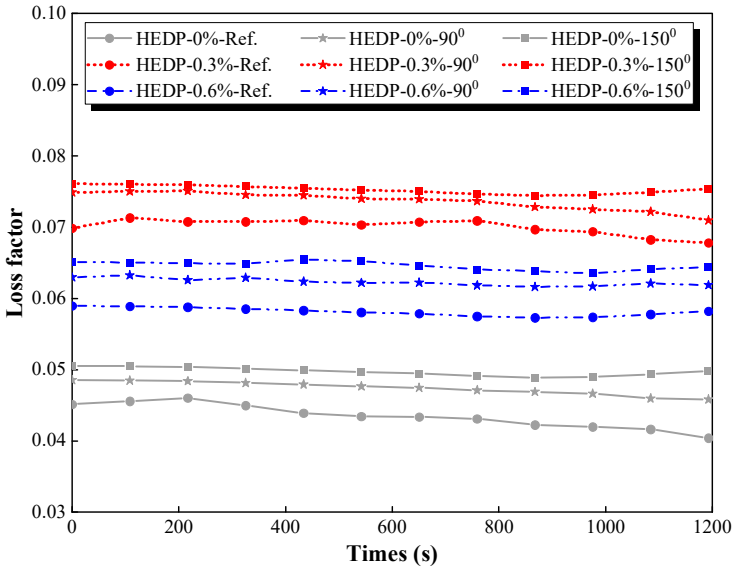

(**b**)

Figure 5. Loss factor of 28d FR-AASC. (**a**) Frequency (0.5–2.5 Hz), (**b**) Time (0–1200 s).

3.5. Storage Modulus of FR-AASC

The variation in storage modulus for FR-AASC samples with frequency from 0.5 to 2.5 Hz and time from 0 to 1200 s is shown in Figure 6. The storage modulus of all FR-AASC samples reached its peak value at 0.5 Hz, as shown in Figure 6a. According to the investigation by Long et al. [14], it was also reported that the coupling effect of dynamic load and temperature resulted in the maximum storage modulus of alkali-activated slag mortar at 0.5 Hz. In addition, the incorporation of HEDP.4Na also showed a significant effect on the storage modulus of the FR-AASC matrix. For a given frequency of 0.5 Hz and the same pouring method, it can be observed that the HEDP-0.3% and HEDP-0.6% increased the storage modulus by 30% and 16%, respectively, compared with the control sample. This was attributed to the fact that an appropriate content of HEDP.4Na led to form more hydration products in the later stage, thereby densifying the internal structure of the matrix and refining the pore size. Lv et al. [54] also reported that 0.04% graphene oxide nanosheets enhanced the storage modulus by 150% of cement paste by regulating the morphology of the cement hydration products and improving the compactness of the microstructure in the cement matrix. However, the enhanced efficiency was weakened in the FR-AASC matrix when the content of HEDP.4Na was over 0.3%.

The pouring method also showed a certain influence on the storage modulus of FR-AASC. For a given excitation frequency of 0.5 Hz and a fixed HEDP.4Na content, the FR-AASC samples cast by 90° and 150° pouring methods increased the storage modulus by 3% and 5%, respectively, compared with the conventional pouring method. Furthermore, the enhanced efficiency of HEDP-0.3% cast by the 150°-induced pouring method increased by 28.8% compared with the reference sample prepared with the conventional pouring method. This was attributed to the fact that the induced pouring method resulted in uniform distribution of steel fibers, reducing the possibility of defects in the matrix [13]. The variation in the storage modulus of FR-AASC was consistent with the 28-day compressive strength tested results.

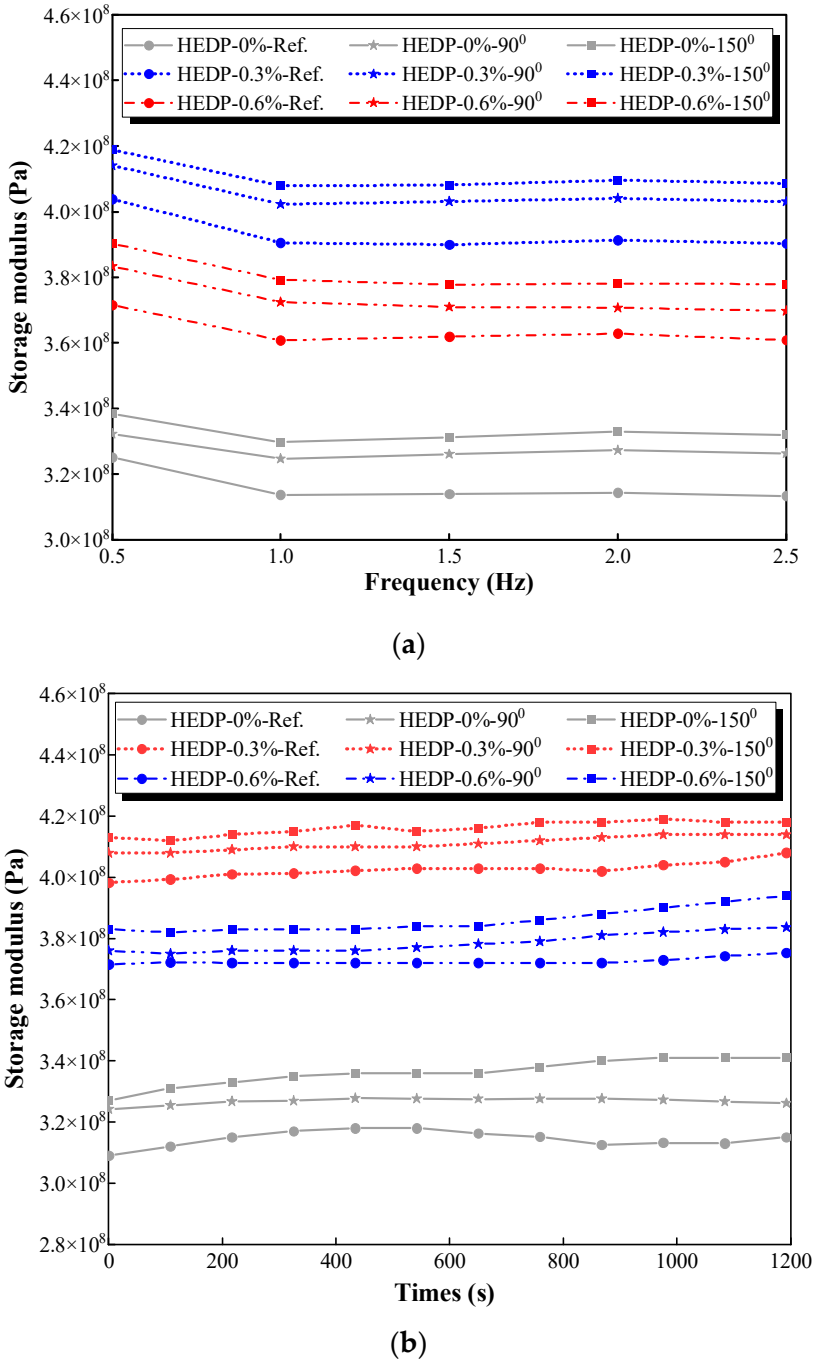

Figure 6. Storage modulus of 28d FR-AASC. (**a**) Frequency (0.5–2.5 Hz), (**b**) Time (0–200 s).

3.6. Phase Analysis

The XRD patterns of FR-AASC mixtures at the age of 3 days are shown in Figure 7. It can be observed that the diffraction peak of C-A-S-H was mainly distributed at 29°. It can be attributed to the fact that the Ca^{2+} chelates with $HEDP^{4-}$ and then precipitates on the surface of the hydration products. The diffraction peaks of hydrotalcite were distributed at 22°, 39°, and 47°, respectively, and the diffraction peaks of calcite in the FR-AASC mixture were distributed at 29°, 39°, 47°, and 49°, respectively. It can be observed that there was no significant difference among the types of crystalline constitutes in FR-AASC specimens incorporated into 0.0%, 0.3%, and 0.6% HEDP.4Na. Therefore, the addition of HEDP.4Na did not change the crystal type of the main hydration products in the FR-AASC sample. In addition, the incorporation content of HEDP.4Na over 0.3% in the FR-AASC

samples inhibited an early polymerization reaction, resulting in a weaker crystallinity of the polymerization products, such as hydrotalcite and C-A-S-H [47]. This can be verified by the difference in intensity of the main diffusion peaks around 22° and 29°. The calcium chelation effect of HEDP.4Na on the dissolved Ca^{2+} ions on the surface of slag particles can inhibit the formation of calcium carbonate, which also verifies that the carbonization of the FR-AASC matrix can slowly form calcite precipitation [49].

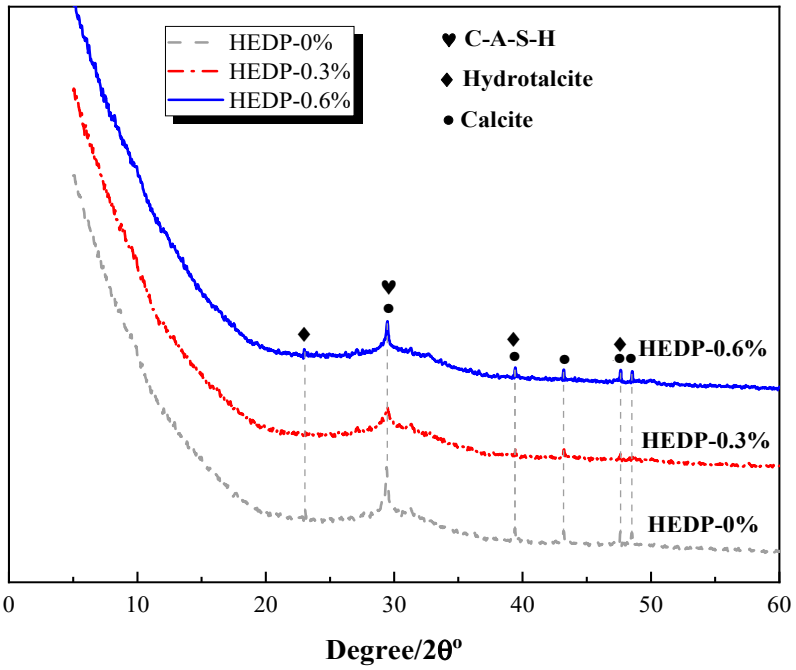

Figure 7. XRD result of 3D FR-AASC.

3.7. Heat of Hydration Analysis

The effect of different HEDP.4Na contents on the characteristics of hydration kinetics at 72 h in the FR-AASC mixture is shown in Figure 8. The hydration process of FR-AASC can be divided into five phases: "the rapid exothermic phase; the dormant stage with low exothermic phase; the hydration acceleration phase; the hydration deceleration stage; and the steady stage" [55]. As shown in Figure 8, the maximum peak of heat flow in the FR-AASC mixture can be significantly reduced and prolonged by the addition of HEDP.4Na. For example, in the hydration acceleration stage, FR-AASC incorporated into 0.3% or 0.6% HEDP.4Na reached the peak value at point D or point F, respectively, compared with the control group at point B. The maximum peak value of the heat flow in the FR-AASC mixture incorporated into 0.3% HEDP.4Na decreased by 51.6%, compared with the reference mixture. This was attributed to the fact that HEDP.4Na inhibited the early polymerization reaction, thus manifesting as a delayed exothermic peak of the early hydration reaction [49]. On the other hand, as shown in Figure 8, it can be observed that the addition of HEDP.4Na can decrease the cumulative heat of hydration compared with the control sample. For example, compared with the FR-AASC mixture without HEDP.4Na (200 $J \cdot g^{-1}$), the peak values of cumulative heat in the FR-AASC mixtures with 0.3% and 0.6% HEDP.4Na were significantly decreased to 90 $J \cdot g^{-1}$ and 80 $J \cdot g^{-1}$, respectively. It was verified that the mini-slump flow of FR-AASC incorporation into HEDP.4Na was higher than that of the reference mixture. HEDP.4Na can prolong the hydration induction period of FR-AASC, which improves the flowability of the mixture and the formation of dense structures in the FR-AASC matrix. This was also verified by the result of the 28-day compressive strength of the FR-AASC samples incorporated with HEDP.4Na.

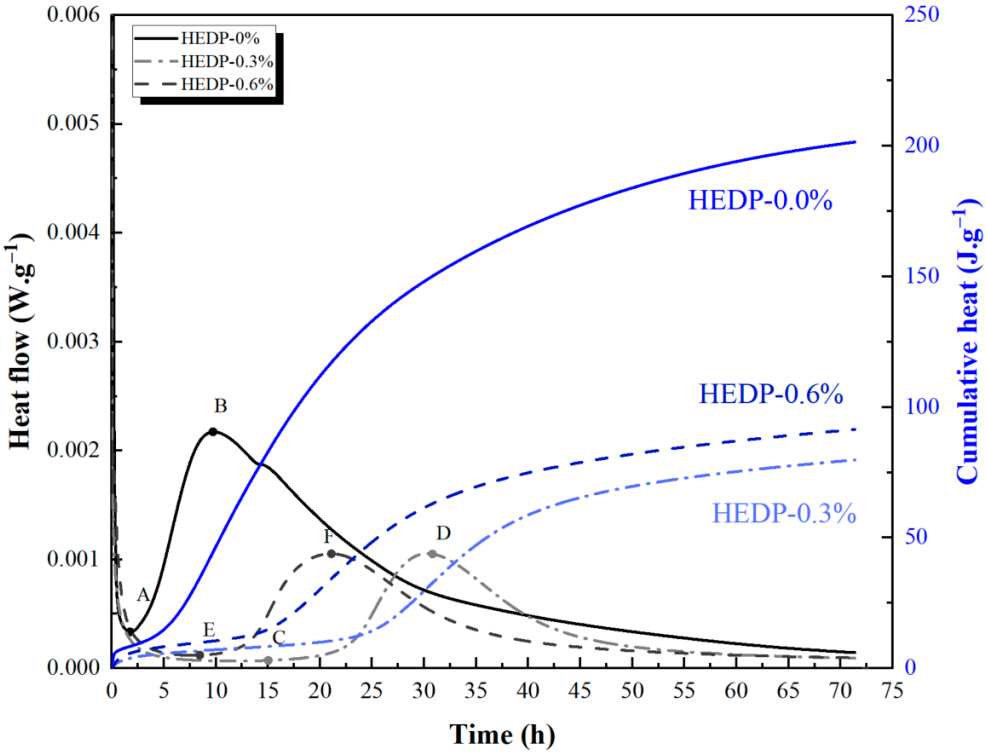

Figure 8. Heat of hydration for AASC.

3.8. Pore Structure Analysis

The mechanical properties (i.e., compressive strength, flexural strength, and damping capacity) of the FR-AASC mixture are influenced by the internal pore microstructure [51]. Figure 9 shows the 28-day total porosity and pore size distribution volume fraction in the FR-AASC sample with or without HEDP.4Na. It can be seen from Figure 9a that the cumulative porosity of the FR-AASC matrix with HEDP.4Na significantly decreased compared with the control sample. The total porosity of FR-AASC incorporated into 0.3% HEDP.4Na was 8%, which is 28% lower than that of the control sample. This was attributed to the fact that the incorporation of HEDP.4Na changed the morphological characteristics of the hydration products, and more macropores or capillary pores in the matrix were partially filled [48,56,57]. The low total porosity in the FR-AASC mixture incorporated into HEDP.4Na improved the 28-day mechanical properties of the matrix compared with the control sample. As shown in Figure 9b, it can be observed that the incorporation of HEDP.4Na led to a significant reduction in the pore size of the FR-AASC matrix. Compared with the control sample, the volume fractions of macropores, macro-capillary pores, and meso-capillary pores in the matrix containing HEDP.4Na slightly decreased, while the volume fraction of mesopores increased. Furthermore, the proportion of gel micropores in the FR-AASC almost kept the same value. The incorporation of 0.3% and 0.6% HEDP.4Na into the FR-AASC matrix resulted in an increase of 18% and 11% in the mesopore volume fraction, respectively. It illustrated that the incorporation of HEDP.4Na modified the shape and size of the hydration products of the FR-AASC matrix, eventually leading to a reduction in larger pores in the AASC matrix.

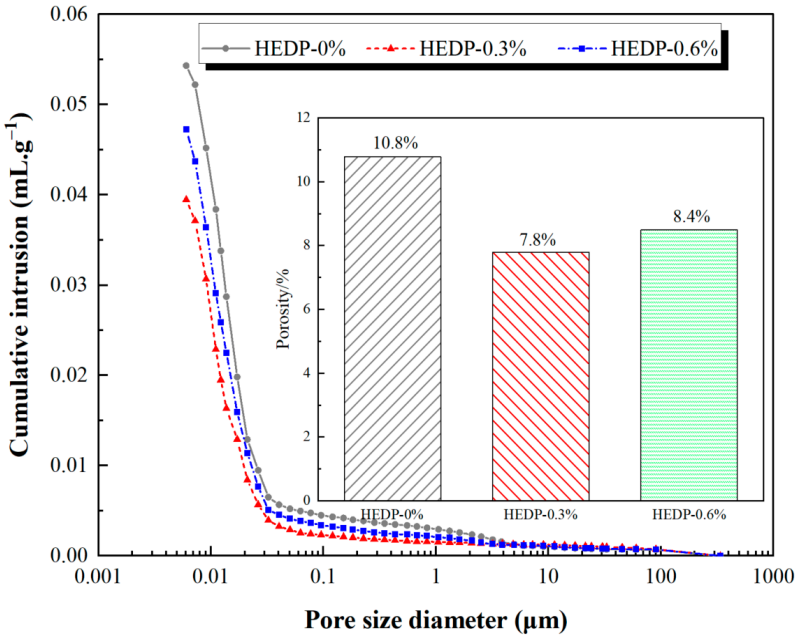

(**a**)

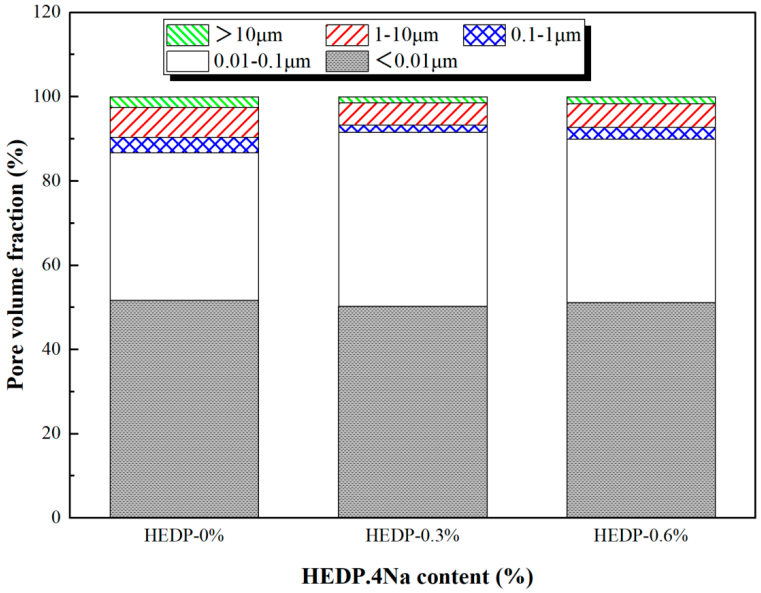

(**b**)

Figure 9. Pore structure of 28d FR-AASC. (**a**) Pore porosity, (**b**) Pore volume fraction.

3.9. Scanning Electron Microscopy (SEM) Analysis

The 28-day microscopic morphology of the FR-AASC samples was observed using SEM to explore the enhanced mechanism of HEDP.4Na on the flexural and damping properties in the FR-AASC mixture. As shown in Figure 10, it can be observed that the FR-AASC matrix incorporated into 0.3% HEDP.4Na showed fewer microcracks and pores than the control group, which may be attributed to the incorporation of HEDP.4Na-decreased porosity of the FR-AASC matrix. On the other hand, it is well known that improvement in the fluidity of the slurry increases the compactness of the FR-AASC matrix. Kiiashko et al. [48] also reported that HEDP could modify the morphology of hydration products through early hydration inhibition, resulting in small-size hydration products and,

ultimately, improving the compactness of the FR-AASC matrix. Therefore, HEDP.4Na can effectively improve the compactness of the FR-AASC matrix and enhance the mechanical properties, which was consistent with the 28-day compressive strength in Section 3.2, flexural strength in Section 3.3, and MIP results in Section 3.8.

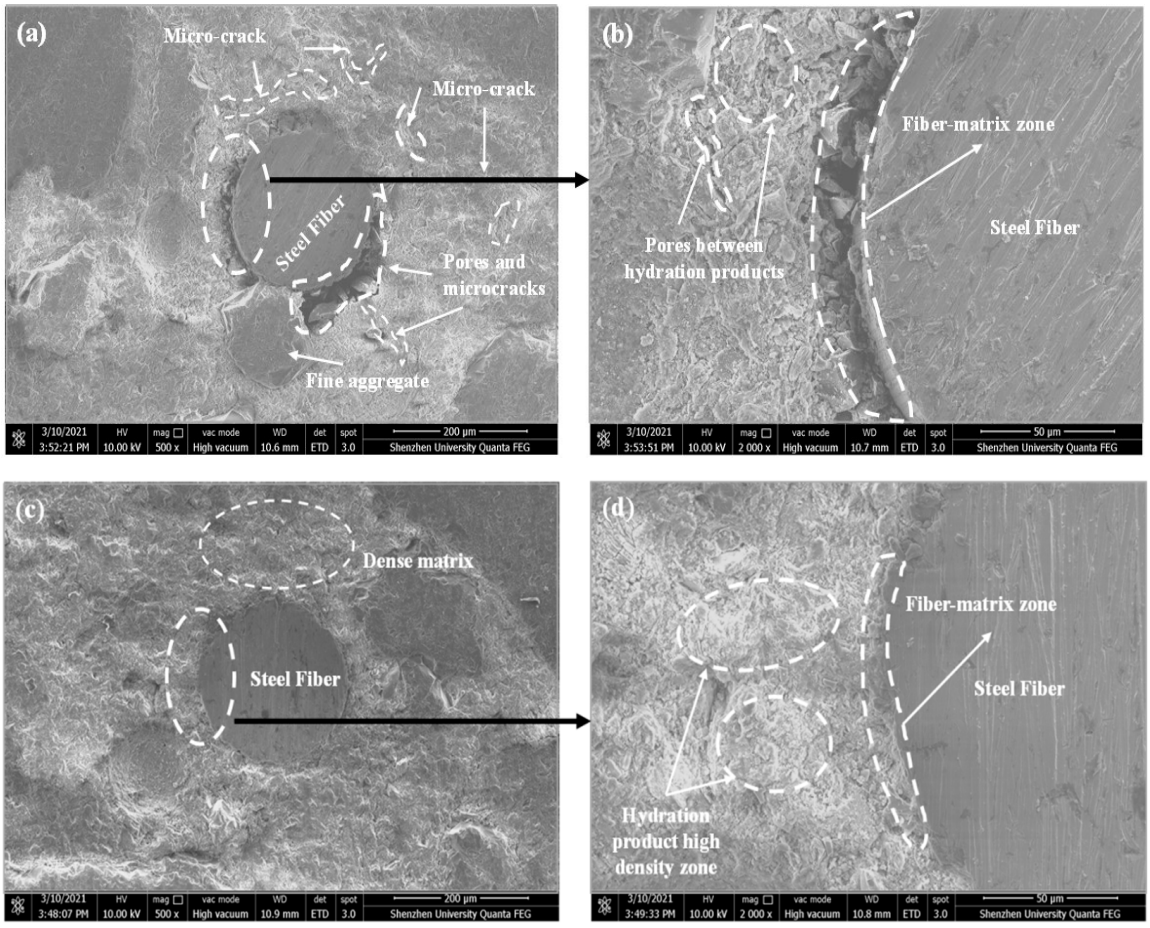

Figure 10. SEM image of 28d FR-AASC: (**a**,**b**) without HEDP.4Na; (**c**,**d**) with addition of 0.3%-HEDP.4Na.

As shown in Figure 10b, the reference sample showed obvious micropores in the fiber–matrix interface transition zone and the weak bonding between the steel fibers and the AASC matrix, compared to FR-AASC with 0.3% HEDP.4Na. The critical shear stress was low as the fiber showed a slip relative to the matrix or was pulled out from the AASC matrix under the external dynamic load. On the contrary, the compactness at the fiber–matrix interfacial transition zone of FR-AASC incorporated into 0.3% HEDP.4Na significantly increased compared with the control sample. The adhesion between the fiber and AASC matrix was improved, and the increase in critical shear stress in the FR-AASC resulted in a high frictional energy dissipation as the fiber–matrix interface was relatively moved. At the same time, the high-density area of hydration products around the fiber–matrix interfacial transition zone can further improve the internal frictional energy dissipation under dynamic load. It was consistent with the results of damping capacity in Section 3.4.

4. Conclusions

This study aimed to investigate the effect of HEDP-4Na content, different pouring methods on compressive and flexural strength, and damping properties of the FR-AASC samples. According to the tested results, the major findings of this study can be summarized as follows:

(1) The FR-AASC sample with HEDP.4Na increased the 28-day compressive and flexural strength by 19% and 17% compared with the control sample. The FR-AASC sample cast by the induced pouring method increased 28-day flexural strength by 42% compared to the sample cast by the conventional method. The synergistic effect of HEDP.4Na and the induced pouring method significantly improved the 28-day flexural strength by 60%.

(2) For a given frequency, the FR-AASC sample with 0.3% and 0.6% HEDP.4Na increased the loss factor by 53% and 30%, respectively, compared to the control group. It was attributed to that HEDP.4Na can modify the fiber–matrix interface transition zone and improve the sliding friction energy dissipation capacity of steel fibers. Compared to the control sample cast by the conventional method, the loss factor of the sample cast by 150°-induced pouring methods increased by 17%. The FR-AASC sample with 0.3% HEDP.4Na cast by the 150°-induced pouring method increased the loss factor by 78% compared with the reference sample prepared with the conventional methodology.

(3) The incorporation of HEDP.4Na and the induced pouring method increased the storage modulus of the FR-AASC matrix. The incorporation of 0.3% HEDP.4Na into samples increased the storage modulus by up to 29% compared with the control sample. Compared to the control sample cast by the conventional method, the storage modulus of FR-AASC samples with HEDP.4Na cast by the 150°-induced pouring method increased by 5.0%.

(4) The use of HEDP.4Na delayed the leaching time of Ca^{2+} and the growth of C-A-S-H, thereby inhibiting the exothermic reaction of hydration in the first 72 h. The total porosity of the sample with HEDP.4Na slightly decreased, which was attributed to the reduction in the size of the hydration products modified by HEDP.4Na. The high-density region of hydration products near ITZ resulted in an improvement in internal frictional energy dissipation under the external dynamic load.

Author Contributions: Conceptualization, J.W. and J.L.; methodology, J.W.; software, J.W.; validation, J.L. and J.W.; formal analysis, J.W.; investigation, J.W.; resources, W.-J.L.; data curation, J.L.; writing—original draft preparation, J.W.; writing—review and editing, W.-J.L. and K.H.K.; visualization, J.W.; supervision, K.H.K.; project administration, W.-J.L.; funding acquisition, W.-J.L. All authors have read and agreed to the published version of the manuscript.

Funding: The authors gratefully acknowledge the financial support provided by the National Natural Science Foundations of China, NSFC-Shandong Joint Fund (No. U2006223), the Science and Technology Project of Shenzhen, China (No. JCYJ20190808151011502), and the Guangdong Provincial Key Research and Development Program (2019B111107003), as well as Advanced Construction and Material Laboratory (ACML) of the Center for Infrastructure Engineering Studies (CIES) at Missouri University of Science and Technology.

Institutional Review Board Statement: Not applicable.

Informed Consent Statement: Not applicable.

Data Availability Statement: Data is contained within the article.

Conflicts of Interest: The authors declare no conflict of interest.

References

1. Prasanna, P.; Srinivasu, K.; Murthy, A.R. Strength and durability of fiber reinforced concrete with partial replacement of cement by ground granulated blast furnace slag. *Mater. Today Proc.* **2021**, *47*, 5416–5425. [CrossRef]
2. Kajaste, R.; Hurme, M. Cement industry greenhouse gas emissions—Management options and abatement cost. *J. Clean. Prod.* **2016**, *112*, 4041–4052. [CrossRef]
3. Lehne, J.; Preston, F. Making Concrete Change Innovation in Low-Carbon Cement and Concrete, Chatham House. Available online: https://policycommons.net/artifacts/1423241/making-concrete-change/2037504/ (accessed on 14 February 2023).
4. Staff, G.C. Forty Cement and Concrete Companies Commit to the Global Cement and Concrete Association's Roadmap to Net Zero. 2021. Available online: https://www.globalcement.com/news/item/13119-forty-cement-and-concrete-companies-commit-to-the-global-cement-and-concrete-association-s-roadmap-to-net-zero (accessed on 14 February 2023).

5. American Society of Civil Engineers (ASCE). 2021 Report Card for a Comprehensive Assessment of America's Infrastructure. 2021. Available online: https://www.infrastructurereportcard.org/wp-content/uploads/2020/12/2021-IRC-Executive-Summary.pdf (accessed on 14 February 2023).
6. P.E.C.C. Group. Capturing Value in the U.S. Cement Industry with a Grinding Plant Utilizing Imported Clinker. 2021. Available online: https://www.penta.net/wp-content/uploads/2021/01/PENTA-Cement-Industry-WhitePaper_Jan2021.pdf (accessed on 14 February 2023).
7. Rashad, A.; Bai, Y.; Basheer, P.; Collier, N.; Milestone, N. Chemical and mechanical stability of sodium sulfate activated slag after exposure to elevated temperature. *Cem. Concr. Res.* **2012**, *42*, 333–343. [CrossRef]
8. Yang, K.-H.; Song, J.-K.; Song, K.-I. Assessment of CO_2 reduction of alkali-activated concrete. *J. Clean. Prod.* **2013**, *39*, 265–272. [CrossRef]
9. Valente, M.; Sambucci, M.; Chougan, M.; Ghaffar, S.H. Reducing the emission of climate-altering substances in cementitious materials: A comparison between alkali-activated materials and Portland cement-based composites incorporating recycled tire rubber. *J. Clean. Prod.* **2022**, *333*, 130013. [CrossRef]
10. Awoyera, P.O.; Adesina, A.; Sivakrishna, A.; Gobinath, R.; Kumar, K.R.; Srinivas, A. Alkali activated binders: Challenges and opportunities. *Mater. Today Proc.* **2020**, *27*, 40–43. [CrossRef]
11. Wu, Y.; Lu, B.; Bai, T.; Wang, H.; Du, F.; Zhang, Y.; Cai, L.; Jiang, C.; Wang, W. Geopolymer, green alkali activated cementitious material: Synthesis, applications and challenges. *Constr. Build. Mater.* **2019**, *224*, 930–949. [CrossRef]
12. Fang, S.; Lam, E.S.S.; Li, B.; Wu, B. Effect of alkali contents, moduli and curing time on engineering properties of alkali activated slag. *Constr. Build. Mater.* **2020**, *249*, 118799. [CrossRef]
13. Long, W.-J.; Wu, Z.; Khayat, K.H.; Wei, J.; Dong, B.; Xing, F.; Zhang, J. Design, dynamic performance and ecological efficiency of fiber-reinforced mortars with different binder systems: Ordinary Portland cement, limestone calcined clay cement and alkali-activated slag. *J. Clean. Prod.* **2022**, *337*, 130478. [CrossRef]
14. Long, W.-J.; Wei, J.-J.; Gu, Y.-C.; Xing, F. Research on dynamic mechanical properties of alkali activated slag concrete under temperature-loads coupling effects. *Constr. Build. Mater.* **2017**, *154*, 687–696. [CrossRef]
15. Zhu, P.; Kai, G.; Kenan, F.; Sanjayan, J.G.; Wenhui, D.; Collins, F. Damping capacity of fly ash-based geopolymer. In Proceedings of the 18th International Conference on Composite Materials (ICCM18), Jeju Island, South Korea, 21–26 August 2011; The Korean Society for Composite Materials: Jeju Island, South Korea, 2011; pp. 1–5. Available online: http://handle.uws.edu.au:8081/1959.7/547489 (accessed on 14 February 2023).
16. Wei, J.; Long, W.-J.; Khayat, K.H.; Dong, B.; Mei, L.; Xing, F. Dynamical properties of environmental high-performance composites with calcined clay. *J. Clean. Prod.* **2021**, *335*, 130226. [CrossRef]
17. Golewski, G.L. A novel specific requirements for materials used in reinforced concrete composites subjected to dynamic loads. *Compos. Struct.* **2019**, *223*, 110939. [CrossRef]
18. Wei, J.; Cheng, B.; Li, L.; Long, W.-J.; Khayat, K.H. Prediction of dynamic mechanical behaviors of coral concrete under different corrosive environments and its enhancement mechanism. *J. Build. Eng.* **2023**, *63*, 105507. [CrossRef]
19. Jinhua, H.; Xing, Z.; Yuanjun, C.; Baisong, Y.; Jian, Z.; Xuemin, W.; Wei, L.; Zhansheng, W.; Ruizhi, Z. Preparation, characterization and application of environment-friendly high density and low damage solid free completion fluids for completing HTHP oil and gas wells. *Geoenergy Sci. Eng.* **2023**, *221*, 211351. [CrossRef]
20. Chi, L.; Lu, S.; Yao, Y. Damping additives used in cement-matrix composites: A review. *Compos. Part B Eng.* **2019**, *164*, 26–36. [CrossRef]
21. Amran, M.; Fediuk, R.; Abdelgader, H.S.; Murali, G.; Ozbakkaloglu, T.; Lee, Y.H. Fiber-reinforced alkali-activated concrete: A review. *J. Build. Eng.* **2021**, *45*, 103638. [CrossRef]
22. Huang, H.; Gao, X.; Li, L.; Wang, H. Improvement effect of steel fiber orientation control on mechanical performance of UHPC. *Constr. Build. Mater.* **2018**, *188*, 709–721. [CrossRef]
23. Jang, S.-J.; Yun, H.-D. Combined effects of steel fiber and coarse aggregate size on the compressive and flexural toughness of high-strength concrete. *Compos. Struct.* **2018**, *185*, 203–211. [CrossRef]
24. Lee, J.-H.; Cho, B.; Choi, E. Flexural capacity of fiber reinforced concrete with a consideration of concrete strength and fiber content. *Constr. Build. Mater.* **2017**, *138*, 222–231. [CrossRef]
25. Swamy, R.N. Fibre reinforcement of cement and concrete. *Mater. Struct.* **1975**, *8*, 235–254. [CrossRef]
26. Huang, H.; Gao, X.; Teng, L. Fiber alignment and its effect on mechanical properties of UHPC: An overview. *Constr. Build. Mater.* **2021**, *296*, 123741. [CrossRef]
27. Wang, C.; Wei, J.; Long, W.-J.; Dong, B. Review on the effect of fiber orientation distribution on mechanical performance of cement-based composites and its evaluated methods. *Mater. Rep.* **2022**, *36*, 20120133. Available online: http://www.mater-rep.com/EN/10.11896/cldb.20120133 (accessed on 14 February 2023).
28. Ferrara, L.; Ozyurt, N.; di Prisco, M. High mechanical performance of fibre reinforced cementitious composites: The role of "casting-flow induced" fibre orientation. *Mater. Struct.* **2011**, *44*, 109–128. [CrossRef]
29. Teng, L.; Huang, H.; Khayat, K.H.; Gao, X. Simplified analytical model to assess key factors influenced by fiber alignment and their effect on tensile performance of UHPC. *Cem. Concr. Compos.* **2021**, *127*, 104395. [CrossRef]
30. Zhang, Y.; Zhu, Y.; Qu, S.; Kumar, A.; Shao, X. Improvement of flexural and tensile strength of layered-casting UHPC with aligned steel fibers. *Constr. Build. Mater.* **2020**, *251*, 118893. [CrossRef]

31. Gou, H.; Zhu, H.; Zhou, H.; Yang, Z. Reinforcement mechanism of orientally distributed steel fibers on ultra-high-performance concrete. *Constr. Build. Mater.* **2021**, *281*, 122646. [CrossRef]
32. Teng, L.; Huang, H.; Du, J.; Khayat, K.H. Prediction of fiber orientation and flexural performance of UHPC based on suspending mortar rheology and casting method. *Cem. Concr. Compos.* **2021**, *122*, 104142. [CrossRef]
33. Zeng, B.; Li, M.; Zhu, Z.; Zhao, J.; Zhang, H. Application of 1-hydroxyethylidene-1,1-diphosphonic acid in boiler water for industrial boilers. *Water Sci. Tech.* **2013**, *67*, 1544–1550. [CrossRef]
34. Liang, H.; Liu, J.; Kang, B.; Zhang, Y.; He, Y.; Yang, H. Optimizing 1-hydroxyethylidene-1,1-diphosphonic acid and mechanically-activated iron ore tailings to prepare low-cost and retarded magnesium oxysulfate cement. *Case Stud. Constr. Mater.* **2022**, *17*, e01631. [CrossRef]
35. Hurnaus, T.; Plank, J. Synthesis, characterization and performance of a novel phosphate-modified fluid loss additive useful in oil well cementing. *J. Nat. Gas Sci. Eng.* **2016**, *36*, 165–174. [CrossRef]
36. Alrefaei, Y.; Wang, Y.-S.; Dai, J.-G. Effect of mixing method on the performance of alkali-activated fly ash/slag pastes along with polycarboxylate admixture. *Cem. Concr. Compos.* **2021**, *117*, 103917. [CrossRef]
37. Raza, A.; El Ouni, M.H.; Azab, M.; Ali, K.; Haider, H.; Rashedi, A. A scientometric review on mechanical and durability performance of geopolymer Paste: Effect of various raw materials. *Constr. Build. Mater.* **2022**, *345*, 128297. [CrossRef]
38. *ASTM C230*; Standard Specification for Flow Table for Use in Tests of Hydraulic Cement. ASTM West Conshohocken: Conshohocken, PA, USA, 2010.
39. *ASTM C403/403M*; Standard Test Method for Time of Setting of Concrete Mixtures by Penetration Resistance. ASTM West Conshohocken: Conshohocken, PA, USA, 2016.
40. *ASTM C109*; Standard Test Method for Compressive Strength of Hydraulic Cement Mortars (Using 2-in. or [50 mm] Cube Specimens). ASTM West Conshohocken: Conshohocken, PA, USA, 2021.
41. *ASTM C 1609*; Standard Test Method for Flexural Performance of Fiber-Reinforced Concrete (Using Beam with Third-Point Loading). ASTM West Conshohocken: Conshohocken, PA, USA, 2019.
42. Long, W.; Fang, C.; Wei, J.; Xu, Z. Study on dynamic properties of alkali-activated cementing materials at different temperatures. In Proceedings of the 2016 7th International Conference on Mechatronics, Control and Materials (ICMCM 2016), Changsha, China, 29–30 October 2016; Atlantis Press: Paris, France, 2016; Volume 104, pp. 75–79. [CrossRef]
43. Long, W.; Wei, J.; Fang, C.; Xiao, B. Analysis on dynamic mechanical properties and surface micro-topography of alkali-activated concrete under different temperatures. In Proceedings of the 2016 International Conference on Materials Science, Resource and Environmental Engineering, Xi'an, China, 6 January 2017; AIP Publishing LLC: Beijing, China, 2017; Volume 1794, p. 020014. [CrossRef]
44. Liu, T.; Song, W.; Zou, D.; Li, L. Dynamic mechanical analysis of cement mortar prepared with recycled cathode ray tube (CRT) glass as fine aggregate. *J. Clean. Prod.* **2017**, *174*, 1436–1443. [CrossRef]
45. Liang, C.; Liu, T.; Xiao, J.; Zou, D.; Yang, Q. The damping property of recycled aggregate concrete. *Constr. Build. Mater.* **2016**, *102*, 834–842. [CrossRef]
46. Sasaki, K.; Kurumisawa, K.; Ibayashi, K. Effect of retarders on flow and strength development of alkali-activated fly ash/blast furnace slag composite. *Constr. Build. Mater.* **2019**, *216*, 337–346. [CrossRef]
47. Ramachandran, V.S.; Lowery, M.S.; Wise, T.; Polomark, G.M. The role of phosphonates in the hydration of Portland cement. *Mater. Struct.* **1993**, *26*, 425–432. [CrossRef]
48. Kiiashko, A.; Chaouche, M.; Frouin, L. Effect of phosphonate addition on sodium carbonate activated slag properties. *Cem. Concr. Compos.* **2021**, *119*, 103986. [CrossRef]
49. Browning, F.H.; Fogler, H.S. Effect of precipitating conditions on the formation of calcium−HEDP precipitates. *Langmuir* **1996**, *12*, 5231–5238. [CrossRef]
50. Teng, L.; Meng, W.; Khayat, K.H. Rheology control of ultra-high-performance concrete made with different fiber contents. *Cem. Concr. Res.* **2020**, *138*, 106222. [CrossRef]
51. Zou, D.; Liu, T.; Teng, J. Improving the damping ability by the addition of Nano SiO_2 to the concrete materials. In Proceedings of the Second International Conference on Smart Materials and Nanotechnology in Engineering, SPEI, Weihai, China, 20 October 2009; pp. 918–926. [CrossRef]
52. Wei, J.-J.; Long, W.-J.; Fang, C.-L.; Li, H.-D.; Guo, Y.-G. Effect of graphene oxide on the damping capability of recycled mortar. In *IOP Conference Series: Materials Science and Engineering, Proceedings of the 4th International Conference on Advanced Engineering and Technology, Shanghai, China, 1 March 2018*; IOP Publishing: Beijing, China, 2018; Volume 317, p. 012001. [CrossRef]
53. Giner, V.T.; Baeza, F.J.; Ivorra, S.; Zornoza, E.; Galao, Ó. Effect of steel and carbon fiber additions on the dynamic properties of concrete containing silica fume. *Mater. Des.* **2012**, *34*, 332–339. [CrossRef]
54. Lv, S.; Ting, S.; Liu, J.; Zhou, Q. Use of graphene oxide nanosheets to regulate the microstructure of hardened cement paste to increase its strength and toughness. *CrystEngComm* **2014**, *16*, 8508–8516. [CrossRef]
55. Sun, J.; Chen, Z. Effect of silicate modulus of water glass on the hydration of alkali-activated converter steel slag. *J. Therm. Anal. Calorim.* **2019**, *138*, 47–56. [CrossRef]

56. Xyla, A.G.; Koutsoukos, P.G. Effect of diphosphonates on the precipitation of calcium carbonate in aqueous solutions. *J. Chem. Soc. Faraday Trans. 1 Phys. Chem. Condens. Phases* **1987**, *83*, 1477–1484. [CrossRef]
57. Tong, S.; Yuqi, Z.; Qiang, W. Recent advances in chemical admixtures for improving the workability of alkali-activated slag-based material systems. *Constr. Build. Mater.* **2021**, *272*, 121647. [CrossRef]